

Growth saturation of unstable thin films on transverse-striped hydrophilic-hydrophobic micropatterns

R. Ledesma-Aguilar,^{1,2} A. Hernández-Machado,¹ and I. Pagonabarraga³

¹*Departament d'Estructura i Constituents de la Matèria. Universitat de Barcelona, Avinguda Diagonal 647, E-08028 Barcelona, Spain*

²*The Rudolf Peierls Centre for Theoretical Physics, University of Oxford, 1 Keble Road, Oxford OX1 2HQ, United Kingdom*

³*Departament de Física Fonamental. Universitat de Barcelona, Avinguda Diagonal 647, E-08028 Barcelona, Spain*

(Dated: November 5, 2018)

Using three-dimensional numerical simulations, we demonstrate the growth saturation of an unstable thin liquid film on micropatterned hydrophilic-hydrophobic substrates. We consider different transverse-striped micropatterns, characterized by the total fraction of hydrophilic coverage and the width of the hydrophilic stripes. We compare the growth of the film on the micropatterns to the steady states observed on homogeneous substrates, which correspond to a saturated sawtooth and growing finger configurations for hydrophilic and hydrophobic substrates, respectively. The proposed micropatterns trigger an alternating fingering-spreading dynamics of the film, which leads to a complete suppression of the contact line growth above a critical fraction of hydrophilic stripes. Furthermore, we find that increasing the width of the hydrophilic stripes slows down the advancing front, giving smaller critical fractions the wider the hydrophilic stripes are. Using analytical approximations, we quantitatively predict the growth rate of the contact line as a function of the covering fraction, and predict the threshold fraction for saturation as a function of the stripe width.

I. INTRODUCTION

The growth of patterns in forced thin liquid films on solid substrates is an ubiquitous process of both biological and technological relevance which has attracted the attention of the scientific community over the last decades [1, 2]. The manipulation of thin films is important in microfluidics, where the increasing miniaturization of fluidic devices demands the development of new and simple ways to handle small volumes of liquid. Due to their smaller internal hydrodynamic resistance and increased surface area, thin films can be used to overcome problems associated to other geometries, such as microchannels [3]. Both experimental and theoretical studies indicate the possibility of using clever structuring of microfluidic devices to orient the growth of films [4–9] or to control the motion of interfaces in confined microfluidic chambers [10].

Still, a remaining challenge is how to control the intrinsic growth of thin liquid films in the microscale. When a thin film of liquid is forced to spread on a dry solid substrate, there is a net accumulation of fluid close to the contact line, which corresponds to the apparent position where the liquid, the solid, and the surrounding gas meet. As a result, the film profile bulges near its leading edge, generating a capillary ridge. For films driven by a body force, such as a constant pressure gradient, variations in the size of the ridge along the leading edge of the film have the effect of increasing the hydrostatic pressure locally. This introduces a driving mechanism that amplifies small perturbations to the contact line, which are relaxed by the surface tension [11]. Such competition of driving and restoring forces gives rise to a linear instability [12–14], which, far from a flat advancing front,

leads to the formation of non-linear structures, such as the familiar water rivulets observed in the shower.

Given the strong interaction with the solid, it is unsurprising that the instability is affected by the wetting properties of the liquid [15–18]. Wetting interactions determine the equilibrium contact angle of the fluid-fluid interface with the solid. As a consequence, the size and shape of the capillary ridge, which control the driving destabilizing force, depend on wetting. For hydrophilic substrates, the contact angle of the interface profile is small, making the capillary ridge relatively thin. The instability is thus weakened [9]. Remarkably, if the size of the ridge is sufficiently small, the restoring capillary pressure is strong enough to balance the driving force after the early stages of growth. The interface thus stops growing, but still retains a curved saturated shape reminiscent of a sawtooth pattern [16]. In contrast, for hydrophobic substrates the net accumulation of mass at the ridge is large enough to outweigh the effect of surface tension, and the emerging film patterns grow steadily, with a shape that resembles that of fingers [17, 18]. Crucially, the lateral lengthscale of the patterns, Λ_{max} , is of the order of the thickness of the thin film. Therefore, in a microfluidic device one expects that the lengthscale of emerging patterns is also of the order of microns.

Our aim in this paper is to demonstrate the exploitation substrate heterogeneity to control the growth of the contact line, up to complete growth saturation. This is appealing to many situations in which fingering is undesirable, for example in coating processes and in ‘chemical channeling’ [3], where the desired lateral lengthscale of the film needs not to be constrained by the intrinsic lengthscale of the instability. We shall thus analyze the effect of a simple, yet effective, substrate pattern

that consists of hydrophilic-hydrophobic stripes oriented transversely to the direction of flow, as shown in Fig. 1. As we shall see below, the lengthscale of the micropattern is important, and has a significant impact already at scales comparable to the micron-sized films. Still, and despite its simplicity, such a pattern has not yet been studied. In a previous study [9], we have demonstrated that the growth of the thin film can be tuned by patterning the solid substrate with transverse or checkerboard arrangements of hydrophilic-hydrophobic domains. Previous experimental and numerical studies of flow patterning [4–7] have mainly focused on the effect longitudinal tracks of varying flow resistance [4] or wetting angle [5–7]. The overall experiments and numerical simulations evidence is that substrate heterogeneity can be used to handle thin films, through preferential orientation over hydrophilic or low-resistance domains in the substrate, or to partially control its growth using checkerboard hydrophilic-hydrophobic patterns. As we shall show in the following, the proposed transverse pattern introduces new physical mechanisms, particularly the transverse spreading of the film, which lead to the desired saturation of the contact line.

Our approach to this problem will be to perform Lattice-Boltzmann (LB) simulations [19] of Navier-Stokes hydrodynamics coupled to a phase-field binary fluid model [20] to account for the interface dynamics. Previous theoretical approaches to model forced thin films on chemically heterogeneous substrates have mainly consisted of sharp-interface formulations based on the Stokes equations [5–8]. Most of these studies use the so-called thin-film equations, which are appropriate to model the fluid dynamics in the limit of small interface slopes. Within this framework, a common procedure to regularize the viscous dissipation singularity is to replace the contact line by a thin precursor film that extends beyond the leading front. The effect of the heterogeneity can then be included by choosing a particular model for the precursor. For example, an heterogeneous disjoining pressure model that couples to the precursor film [7] has been used to study the motion of the film on longitudinal-stripped and disordered substrates, as well as on ordered and disordered isolated spots [8]. Alternatively, a similar model consisting of a spatially-varying thickness of the precursor film to study the motion of the film over chemical patterns has also been used [5, 6].

Our aim in this work is to study the effect of a sharp contrast between hydrophilic and hydrophobic domains in the proposed micropatterns. This corresponds to situations in which the static and dynamic contact angles need not to be small. Such regime falls beyond the limit of applicability of the thin-film equations, demanding the resolution of the full three-dimensional dynamics. This is a complicated problem from the classical point of view, as it involves the motion of two free boundaries: the film surface and the contact line. Within sharp-interface formulations, boundary integral methods could be used to address this problem, as has been done to model the effect

of chemical heterogeneities on two-dimensional fluid nanodrops [21]. However, the mesoscopic approach that we take here constitutes a reliable three-dimensional Navier-Stokes solver that allows for both small and large contact angles, necessary to model hydrophilic and hydrophobic interactions. Because of the diffuse approximation to describe the fluid interface, the method circumvents the free-boundary problem, regularizes the viscous dissipation singularity at the contact line, and deals naturally with merging and pinch-off events, which otherwise need a specific rule in sharp interface approximations. We have carried out a validation of our model in a previous study, for the case of driven thin films on homogeneous solid substrates [22].

The rest of this work is organized as follows. In Section II we introduce the mesoscopic model and the Lattice-Boltzmann algorithm to perform the numerical simulations. We will complement our numerical results with kinematical calculations for the propagation of the interface. As we shall see from our numerical results, presented in Section IV, the main effect of the transverse hydrophilic stripes on the forced film is to favor its lateral spreading on hydrophilic domains, thus slowing down the leading edge of the film. The same lateral spreading ultimately leads to a speed-up of the trailing edge of the film. The net result is that the growth rate of the film decreases with increasing fraction of hydrophilic stripes in the substrate, until the film saturates above a critical value of this fraction. As we detail in the discussion and conclusions of this work, presented in Section V, we predict that a relatively small fraction of hydrophilic stripes is sufficient to suppress the growth of the contact line in experimental realizations. Our results thus constitute a promising step towards the control of interface growth in microfluidic systems.

II. MODEL

In this paper we shall perform numerical simulation of Navier-Stokes level hydrodynamics coupled to a phase-field representation of the viscous fluid film and surrounding low-viscosity phase. Such modeling is very useful to address the dynamics of immiscible fluids, as it has the advantage of circumventing the free-boundary problem associated to sharp-interface representations, as for example in boundary integral methods. Furthermore, the phase-field model regularizes the viscous dissipation singularity at the contact line through a diffusive mechanism acting at small scales (of the order of the size of the interface). One thus does not need to specify additional boundary conditions at the contact line. In order to integrate the model equations, we will use a Lattice-Boltzmann algorithm.

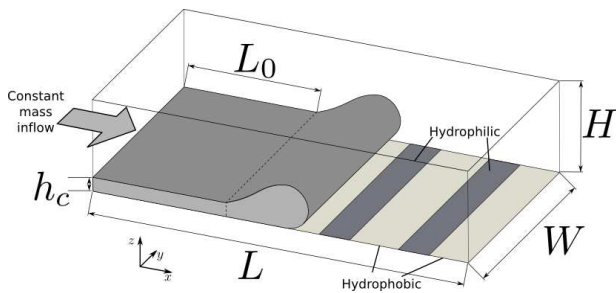


FIG. 1: Schematic representation of the system. A thin film of initial thickness h is forced along the x direction by the action of a constant body force, \vec{f} , on a solid substrate composed of hydrophilic and hydrophobic transverse stripes. The scale of the thin film thickness and of the width of the stripes is of the order of microns.

A. Hydrodynamics and Phase-Field Model

A schematic depiction of the forced thin-film geometry is presented in Fig. 1. We consider two immiscible Newtonian fluids of viscosities η_1 and η_2 and densities ρ_1 and ρ_2 , respectively. The thin film, corresponding to fluid 1, is forced on a solid substrate composed of hydrophilic and hydrophobic regions. In order to distinguish between the two liquids, we introduce a phase field characterized by a concentration variable, or order parameter, ϕ . The local value of the order parameter thus describes each phase, and varies between two volume values across a diffuse interfacial region.

In equilibrium, the free energy of the system can be written as a functional of the order parameter field, $\phi(\vec{r})$ and the local density field, $\rho(\vec{r})$,

$$\mathcal{F}\{\rho, \phi\} = \int_V dV \left(U(\phi, \rho) + \frac{\kappa}{2} (\vec{\nabla}\phi)^2 \right) + \int_S dS f_S(\phi_S). \quad (1)$$

The first integral in Eq. (1) is composed by the volume contributions to the free energy. These consist of a double-well potential with an ideal gas term, $U(\phi, \rho) = A\phi^2/2 + B\phi^4/4 + (1/3)\rho \ln \rho$, and a square-gradient term that penalizes variations of the order parameter, thus allowing for the formation of a diffuse interface. The parameters A , B and κ control the equilibrium values of the order parameter $\pm\phi_{\text{eq}} = \pm\sqrt{-A/B}$, the size of the interface, $\xi = \sqrt{-\kappa/2A}$ and the fluid-fluid surface tension, $\gamma = \sqrt{-8\kappa A^3/9B^2}$. The second integral in the free energy corresponds to the contribution of fluid-solid interactions. Here we chose a Chan model, $f_S(\phi_S) = C\phi_S$, which assigns the free surface energy f_S according to the local value of the order parameter at the boundary, ϕ_S . The parameter C controls the equilibrium contact angle, θ_e , of the fluid-fluid interface in contact with a flat solid

wall through the relation

$$\cos \theta_e = \frac{1}{2} \left[- \left(1 - C(-\kappa A)^{-\frac{1}{2}} \right)^{\frac{3}{2}} + \left(1 + C(-\kappa A)^{-\frac{1}{2}} \right)^{\frac{3}{2}} \right]. \quad (2)$$

The order parameter and density fields contribute to the chemical potential, μ , and pressure tensor, $P_{\alpha\beta}$, of the system. These are obtained by taking functional derivatives of the free energy [23] and have the following expressions,

$$\mu = A\phi + B\phi^3 - \kappa\nabla^2\phi, \quad (3)$$

$$P_{\alpha\beta} = \left(\frac{1}{3}\rho + \frac{1}{2}A\phi^2 + \frac{3}{4}B\phi^4 - \kappa\phi\nabla^2\phi - \frac{1}{2}\kappa|\vec{\nabla}\phi|^2 \right) \delta_{\alpha\beta} + \kappa(\partial_\alpha\phi)(\partial_\beta\phi). \quad (4)$$

Out of equilibrium, the dynamics of the density, ρ , velocity, \vec{v} , and order parameter, ϕ , fields are given by the continuity and Navier-Stokes equations, plus a convection-diffusion equation for the phase field, *i.e.*,

$$\frac{\partial\rho}{\partial t} + \vec{\nabla} \cdot (\rho\vec{v}) = 0, \quad (5)$$

$$\frac{\partial\vec{v}}{\partial t} + (\vec{v} \cdot \vec{\nabla})\vec{v} = -\vec{\nabla}P - \phi\vec{\nabla}\mu + \eta\nabla^2\vec{v} + \vec{f}, \quad (6)$$

and

$$\frac{\partial\phi}{\partial t} + \vec{v} \cdot \vec{\nabla}\phi = M\nabla^2\mu, \quad (7)$$

respectively.

The ϕ -dependent term in the Navier-Stokes equations arises from the concentration dependence of the pressure tensor in Eq. (4), giving a ‘chemical’ force density, $-\phi\vec{\nabla}\mu$, which plays a similar role as the pressure gradient term in the volume of each phase. The remaining terms in the Navier-Stokes equations are the viscous friction term, whose strength is controlled by the local viscosity, η , and to the body force term, \vec{f} .

The evolution of the order parameter is dictated by Eq. (7), which contains an advective term caused by the underlying velocity field and a diffusive term, whose strength is controlled by the mobility parameter M .

B. System Geometry and Boundary Conditions

In order to ensure the formation of steady patterns, we choose a constant flux configuration for the geometry of the system. We set a rectangular simulation domain of linear dimensions $L \times W \times H$, in the x , y and z directions, respectively. The solid-fluid interface, S , is parallel to the $x-y$ plane and located at $z=0$ as shown in Fig. 1. The thin film is initially at rest and occupies the volume $V_0 = L_0 \times W \times h_c$. We fix the

force term as $\vec{f} = \frac{1}{2}f_x(\phi + 1)\hat{x}$, so fluid 1 is forced uniformly while fluid 2 is left to evolve passively. This sets up a flow of mean velocity $u = h_c^2 f_x / 3\eta_1$ within the film. At $x = 0$, a constant flux in the x direction is thus ensured as long as there is a reservoir of fluid available to compensate for the downstream motion of the film. This is achieved by imposing $\partial_x \rho(x = \{0, L\}, y, z) = 0$, $\partial_x \vec{v}(x = \{0, L\}, y, z) = \vec{0}$ and $\partial_x \phi(x = \{0, L\}, y, z) = 0$. Using this approach, we do not find any appreciable variations of the mean velocity of the film or the film thickness close to the boundary.

We fix periodic boundary conditions in the y direction, *i.e.*, $\rho(x, y = W, z) = \rho(x, y = 0, z)$, $\vec{v}(x, y = W, z) = \vec{v}(x, y = 0, z)$, $\phi(x, y = W, z) = \phi(x, y = 0, z)$. At the upper boundary, a shear-free boundary condition is imposed by fixing $\partial_z \vec{v}(x, y, z = H) = \vec{0}$, while vanishing density and concentration gradients normal to the boundary are fixed by imposing $\partial_z \rho(x, y, z = H) = 0$ and $\partial_z \phi(x, y, z = H) = 0$.

The velocity profile is subject to stick boundary and impenetrability conditions at the solid-fluid surface, *i.e.*,

$$\vec{v}|_S = 0. \quad (8)$$

In macroscopic representations, imposing the stick boundary condition for a moving interface in contact with a solid causes a spurious divergence of the viscous stress as one approaches the contact line [24]. This paradox is readily avoided by the phase-field model, through the diffusive term in Eq. (7), which allows for a slip velocity that increases as one approaches the contact line [25], even when Eq. (8) is enforced. Diffusion is driven by variations of the chemical potential profile close to the contact line, over a typical lengthscale l_d , which scales as $l_d \sim (\eta_1 \xi M / \Delta \phi^2)^{1/4}$ [26].

An evolution equation for the order parameter should be specified at the solid-fluid interface (see [25] for a detailed derivation). In this paper we shall impose the natural boundary condition

$$\hat{n} \cdot \vec{\nabla} \phi|_S = \frac{1}{\kappa} \frac{df_S}{d\phi_S}. \quad (9)$$

This gives an instantaneous relaxation of the order parameter gradient to its surface value at the wall, which corresponds to quasi-equilibrium dynamics for the interface slope at lengthscales comparable to the size of the interface [27]. By choosing the wetting parameter C in Eq. (2), we specify the local value of the equilibrium contact angle and hence the desired hydrophilic-hydrophobic pattern.

The ϕ -dependent term in Eq. (6) is most important at the fluid-fluid interface, where it plays the role of a Laplace pressure. This behavior can be verified by integration of Eq. (6) over the length of the interface (c.f. [28]) whence one recovers a jump in the normal stress

$$\Delta \mu \sim \frac{\gamma}{R}. \quad (10)$$

Eq. (10) corresponds to the Young-Laplace condition with R being the local radius of curvature of the interface. Thus, the concentration dependent term in the Navier-Stokes equation eliminates the need of using Eq. (10) explicitly. Accordingly, the continuity of the tangential stress is recovered in the sharp interface limit.

In order to present our results in a natural scale, we choose units according to the classical thin-film theory in the lubrication limit [1, 2]. For microscales inertial effects are negligible, and the relevant control parameter is the capillary number, $Ca = \eta_1 u / \gamma$, which measures the ratio of viscous to capillary forces. A suitable unit system is

$$x^* = \frac{x}{x_c}, \quad y^* = \frac{y}{x_c}, \quad (z^*, h^*) = \left(\frac{z}{h_c}, \frac{h}{h_c} \right),$$

$$\langle \vec{v} \rangle^* = \frac{\langle \vec{v} \rangle}{u}, \quad \text{and} \quad \frac{t}{t_c}, \quad (11)$$

where $x_c = h_c(3Ca)^{-\frac{1}{3}}$, and $t_c = x_c/u$.

C. Parameter values

The model presented in the previous section is specified by a set of parameters, $\rho_1, \rho_2, \eta_1, \eta_2, \phi_{\text{eq}}, \gamma, \xi$ and M . Additionally, the fluid wetting properties are specified by the static contact angle, θ_e , which depends on C . In the following, we specify the values of these parameters used in our simulations (all in lattice units).

The equilibrium values of the order parameter are fixed to $\phi^* = \pm 1$ by choosing $A = -B$. To specify the viscosity of each fluid we fix the mean viscosity $\langle \eta \rangle = 0.1$ and the viscosity contrast, $\delta \eta = 0.9$. The local viscosity, $\eta(\vec{r})$, is then set as $\eta_1 = \langle \eta \rangle(1 + \delta \eta)$ if $\phi > 0$ (viscous film) and $\eta_2 = \langle \eta \rangle(1 - \delta \eta)$ if $\phi < 0$ (surrounding low-viscosity phase). The density is set to the same mean value in each phase, $\rho_1 = \rho_2 = 1$. The fluid-fluid surface tension is fixed to $\gamma = 2.3 \times 10^{-3}$. The interface width is set to $\xi = 0.57$, which corresponds to an effective transition zone of ~ 5 lattice spacings for the order parameter profile between the volume values in equilibrium.

In order to ensure that the contact line propagates with a velocity comparable to the velocity of the film [22], we fix the mobility to $M = 10.0$.

The equilibrium contact angles used throughout this study correspond to $\theta_e = 0^\circ$ for the *hydrophilic* substrate and $\theta_e = 90^\circ$ for the *hydrophobic* substrate, which corresponds to $C = 0$ and $C = 1.7 \times 10^{-3}$, respectively.

The capillary number is set to $Ca = 0.41$, which follows from choosing the forcing f_x to give a mean velocity value for the film, $u = 0.005$. This value ensures the stability of the LB scheme and a small compressibility (density variations of the order of $\sim 1\%$.)

III. LATTICE BOLTZMANN METHOD

We use the Lattice-Boltzmann (LB) implementation introduced in detail in Ref. [23, 29] in the context of spinodal decomposition of binary fluid mixtures, and which we have used in a previous work [9], where we have focused on the dynamics of unstable thin films in homogeneous solid substrates. In LB, the dynamics are introduced by two sets of velocity distribution functions, f_i and g_i , which evolve in time according to the discretized Boltzmann equations,

$$f_i(\vec{r} + \vec{c}_i, t + 1) - f_i(\vec{r}, t) = -\frac{1}{\tau_f}(f_i - f_i^{eq}) + F_i^f, \quad (12)$$

and

$$g_i(\vec{r} + \vec{c}_i, t + 1) - g_i(\vec{r}, t) = -\frac{1}{\tau_g}(g_i - g_i^{eq}), \quad (13)$$

Space is discretized as a cubic lattice where nodes are joined by velocity vectors, \vec{c}_i . Here we use the D3Q19 model, which consists of a set of 19 velocity vectors in three dimensions [23]. Hence, f_i and g_i are proportional to the number of particles moving in the direction of \vec{c}_i . Eqs. (12) and (13) are composed of two steps. First, the distribution functions are relaxed to their equilibrium values, represented by f_i^{eq} and g_i^{eq} , with relaxation timescales τ_f and τ_g . The term F_i^f is related to the external forcing. Following this collision stage, distribution functions are propagated to neighboring sites.

The mapping between LB scheme and the hydrodynamic phase-field model is done by defining the hydrodynamic variables through moments of the f_i and g_i . The local density and order parameter are given by $\sum_i f_i = \rho$ and $\sum_i g_i = \phi$, while the fluid momentum and order parameter current are defined as $\sum_i f_i \vec{c}_i = \rho \vec{v}$ and $\sum_i g_i \vec{c}_i = \phi \vec{v}$.

Local conservation of mass and momentum is enforced through the conditions $\sum_i f_i = \sum_i f_i^{eq} = \rho$, $\sum_i g_i = \sum_i g_i^{eq} = \phi$, $\sum_i f_i \vec{c}_i = \sum_i f_i^{eq} \vec{c}_i = \rho \vec{v}$ and $\sum_i g_i \vec{c}_i = \sum_i g_i^{eq} \vec{c}_i = \phi \vec{v}$. In equilibrium, the pressure tensor and chemical potential are defined as $\sum_i f_i^{eq} \vec{c}_i \vec{c}_i = \rho \vec{v} \vec{v} + \bar{P}_T$ and $\sum_i g_i^{eq} \vec{c}_i \vec{c}_i = \hat{M} \mu \bar{\delta} + \phi \vec{v} \vec{v}$.

To recover the equilibrium behavior of the phase-field model, the equilibrium distribution functions and the forcing term are expanded in powers of \vec{v} [30], *i.e.*,

$$f_i^{eq} = \rho \omega_\nu \left(A_\nu^f + 3\vec{v} \cdot \vec{c}_i + \frac{9}{2} \vec{v} \vec{v} : \vec{c}_i \vec{c}_i - \frac{3}{2} v^2 + \bar{G}^f : \vec{c}_i \vec{c}_i \right),$$

$$g_i^{eq} = \rho \omega_\nu \left(A_\nu^g + 3\vec{v} \cdot \vec{c}_i + \frac{9}{2} \vec{v} \vec{v} : \vec{c}_i \vec{c}_i - \frac{3}{2} v^2 + \bar{G}^g : \vec{c}_i \vec{c}_i \right)$$

and

$$F_i^f = 4\omega_\nu \left(1 - \frac{1}{2\tau_f} \right) \left[\vec{f} \cdot \vec{c}_i (1 + \vec{v} \cdot \vec{c}_i) - \vec{v} \cdot \vec{f} \right].$$

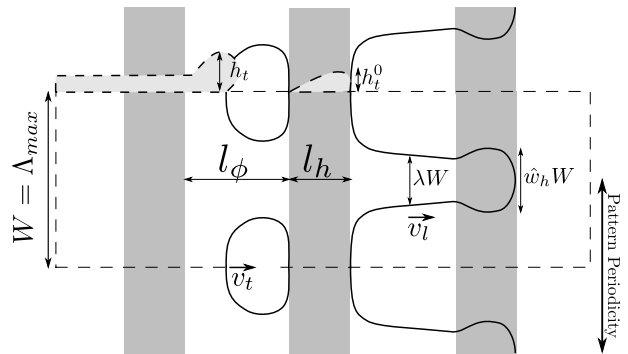


FIG. 2: Geometry of the transverse stripe pattern. The pattern is composed of alternated hydrophilic (grey) and hydrophobic (white) stripes of lengths l_h and l_ϕ , respectively. The panel shows a schematic representation of the contact line (solid line), which spreads on the hydrophilic stripes up to a width $\hat{w}_h W$ before advancing on the next hydrophobic stripe. Spreading causes that a series of dry spots are left on the hydrophobic stripes, which are eventually covered by the trailing edge of the film. The dotted lines depict the thin film profile, which has a typical thickness h_t^0 on a wet hydrophilic stripe, and a maximum thickness h_t at the trailing edge on a hydrophobic stripe. At the grey zones $\theta_e = 0^\circ$ while at the white zones $\theta_e = 90^\circ$.

Here, ν stands for the three possible magnitudes of the \vec{c}_i set. The values of the coefficients are then fixed by the definition of the moments of f_i^{eq} and g_i^{eq} , and by the symmetry of the lattice. Coefficient values for the D3Q19 LB scheme are $\omega_0 = 2/9$, $\omega_1 = 1/9$ and $\omega_{\sqrt{3}} = 1/72$; $A_0^f = 9/2 - 7/2 \text{Tr} \bar{P}$, $A_1^f = A_{\sqrt{3}}^f = 1/\rho \text{Tr} \bar{P}$ and $\bar{G}^f = 9/(2\rho) \bar{P} - 3\bar{\delta} \text{Tr} \bar{P}$; $A_0^g = 9/2 - 21/2 \hat{M} \mu$, $A_1^g = A_{\sqrt{3}}^g = 3\hat{M} \mu / \rho$ and $\bar{G}^g = 9/(2\rho) \hat{M} \mu (\bar{1} - \bar{\delta})$, where $\bar{1}$ is the unit matrix.

The hydrodynamic phase-field model, given by Eqs. (5), (6) and (7), up to second order corrections in the velocity, can be recovered by performing a Chapman-Enskog expansion of Eqs. (12) and (13)[30]. The LB scheme maps to the hydrodynamic model through the relaxation timescales, *i.e.*, $\eta = (2\tau_f - 1)/6$ and $M = (\tau_g - 1/2)\hat{M}$, and through the body force $\vec{f} = \rho \vec{g}$.

Solid boundaries in the Lattice-Boltzmann method are implemented by means of the well known bounce-back rules[30, 31]. In the lattice nodes that touch the solid, the propagation scheme is modified so the distribution functions are reflected to the fluid rather than absorbed by the solid. As a consequence, a stick condition for the velocity is recovered approximately halfway from the fluid node to the solid node.

IV. RESULTS

We want to assess if a small fraction of hydrophilic domains can induce a significant reduction of the growth of the contact line. We thus characterize the trans-

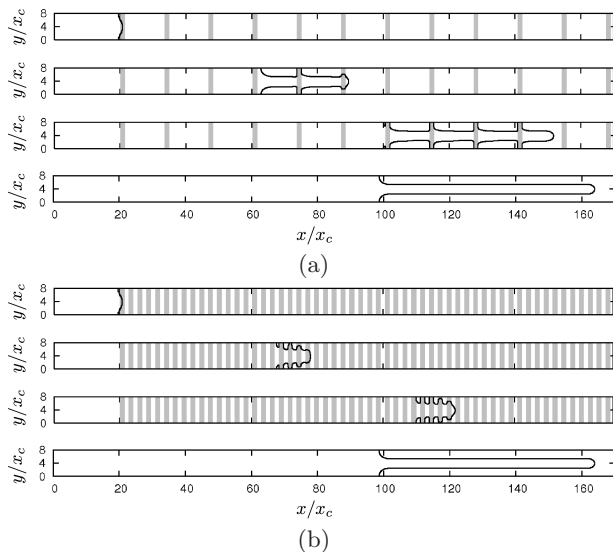


FIG. 3: Contact line evolution on transverse stripe patterns for hydrophilic stripes of length $l_h/x_c = 1.3$ at different covering fraction, f . The first panel in each figure shows the initial perturbation at $t/t_c = 0$, while the subsequent two panels show the contact line at time intervals of $\Delta t/t_c = 67$. For comparison, the last panel in (a) and (b) shows the finger that grows on a homogeneous hydrophobic substrate ($f=0$) at $t = 2\Delta t/t_c$. For both values of f , the contact line grows as a finger on the hydrophobic stripes, and spreads transversely on the hydrophilic domains. (a) For a small fraction of hydrophilic stripes, $f = 0.11$, the contact line grows at a smaller rate than the one measured on a homogeneous substrate. (b) Increasing the fraction to $f = 0.55$ has the effect of decreasing the growth rate dramatically, making the length of the contact line substantially smaller than the length of the unperturbed finger. As seen by comparing the position of the contact line in third panel of (a) and (b), the reduction of the growth rate arises both from a slow down of the leading edge and a speed up of the trailing edge of the contact line.

verse stripe arrangement by the width of the hydrophilic stripes, l_h , and the fraction of the substrate that is covered by them, $f = l_h/(l_h + l_\phi)$, where l_ϕ is the length of the hydrophobic stripes, as depicted in Fig. 2.

In a previous study [9], we have considered the motion of thin films on homogeneous substrates. We have found that the front develops as a finger if the substrate is hydrophobic ($\theta_e = 90^\circ$), with an inter-finger spacing given by $\Lambda_{max}(\theta_e = 90^\circ) \simeq 8x_c$. In contrast, for a hydrophilic substrate the front develops as a sawtooth with a typical lateral lengthscale of $\Lambda_{max}(\theta_e = 0^\circ) \simeq 14x_c$. Due to the periodicity of the emerging structures, it is sufficient to consider simulation domains of width $W = \Lambda_{max}(\theta_e = 90^\circ) \simeq 8x_c$. Larger system sizes obeying $W = n\Lambda_{max}(\theta_e = 90^\circ)$, with n being an integer, only give rise to additional identical fingers, whose effect is already taken into account by the periodic boundary conditions in our simulations. For non-integer n we expect a non-linear competition of emerging fingers, which we have observed previously [9]. However, this compe-

tion should not modify significantly the main effect of the transverse-stripe pattern.

In the following, we will explore the dynamics of the front when varying l_h and f . We study the effect of the occupation fraction in the range $0 \leq f \leq 1$, while for the length of the stripes we choose the values $l_h/x_c = 1.3$, $l_h/x_c = 4.0$, and $l_h/x_c = 6.7$. As before, we consider the evolution of a single mode in systems whose width is chosen to be close to the most unstable wavelength predicted for the hydrophobic substrate.

Figures 3(a) and 3(b) show the evolution of the contact line for $f = 0.11$ and $f = 0.55$ respectively, for a stripe width $l_h/x_c = 1.3$ at three subsequent times, $t_0/t_c = 0$, $t_1/t_c = 67$ and $t_2/t_c = 134$. For comparison, the last panel at the bottom of (a) and (b) shows the interface profile for a homogeneous hydrophobic substrate ($f=0$) at $t_2/t_c = 134$. The main feature in these patterns is that the growth rate of the contact line decreases strongly as the fraction of hydrophilic stripes is increased. For the value of l_h considered in Fig. 3, the growth rate actually vanishes at a critical fraction $f_c \simeq 0.59$. We first notice that for both patterns shown in Fig. 3, the leading edge of the contact line grows as a finger when it is in contact with a hydrophobic stripe. The finger grows until it touches a hydrophilic stripe, where it starts to spread transversely. As spreading takes place, the leading edge continues advancing over the hydrophilic domain, until it reaches the next hydrophobic stripe, where it develops as a finger again. A closer inspection of Fig. 3(a) shows that a series of spots are left uncovered momentarily on the hydrophobic stripes after the leading edge has passed by. This is a consequence of the transverse spreading process that occurs every time the leading edge passes over a hydrophilic stripe. The second and third panels in Fig. 3(a) show that the trailing spot is eventually covered by the film, and that only after the trailing spot has disappeared, the following spot starts to be covered. This mechanism holds for larger f , as can be seen in Fig. 3(b). The global result is that the transverse pattern induces a slow down of the leading edge, as can be seen by comparing the contact line with the finger that grows on a homogeneous substrate. This effect is stronger for $f = 0.55$ than for $f = 0.11$. Additionally, the transverse pattern induces a speed up of the trailing edge, and effect that can also clearly be seen in Fig. 3. Again, this effect is stronger the larger f is.

The combination of the speed up of the trailing edge and the slow down of the leading edge causes the contact line growth rate, \dot{L} , to decrease with increasing fraction of hydrophilic stripes. Figure 4 shows a plot of \dot{L} as a function of f . The limits in this plot correspond to the finger ($f = 0$) and sawtooth ($f = 1$) solutions on homogeneous substrates. For small f , the growth rate converges to the growth rate of the unperturbed finger, while increasing f has the effect of decreasing the growth rate as explained above. We find that \dot{L} vanishes at a critical fraction, $f_c(l_h)$, which is considerably smaller than unity. This means that the transverse pattern induces the saturation

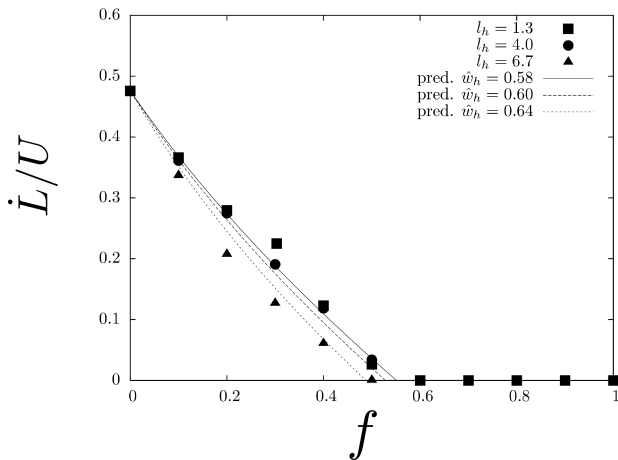


FIG. 4: Global contact line growth rate as a function of the fraction of hydrophilic stripes for different hydrophilic stripe lengths on transverse striped patterns. The growth rate \dot{L} , decreases as the fraction of hydrophilic stripes, f , increases. For fixed f , increasing the length of the hydrophilic stripes, l_h , has the effect of decreasing the growth rate. Continuous lines correspond to the kinematical theoretical prediction, for which the dependence on l_h is contained in the parameter \hat{w}_h , which we measure from simulations. The plot shows that the growth rate vanishes at a fraction that is smaller than unity.

of the contact line by caused by transverse spreading of the film on hydrophilic domains.

To analyze the effect of the length of the stripes, l_h , we have carried out additional simulations at fixed f while varying l_h and have measured the corresponding growth rate. We plot these results in Fig. 4, where we observe that the growth rate decreases systematically as l_h is increased. Accordingly, the critical fraction $f_c(l_h)$ is a decreasing function of l_h .

Analytical model for growth on transverse stripe patterns

In order to gain insight into the growth of the contact line on transverse patterns, we will analyze the interplay between hydrophilic and hydrophobic stripes using a kinematical argument.

Let us denote Δt_l and Δt_t the time intervals in which the leading and trailing edges sweep a distance $\Delta l = l_\phi + l_h$, respectively. For a mean steady growth of the interface, each of these intervals can be decomposed as the sum of the time that the interface spends on a hydrophilic and a hydrophobic stripe. We thus write

$$\Delta t_l = \Delta t_l^h + \Delta t_l^\phi \quad \text{and} \quad \Delta t_t = \Delta t_t^h + \Delta t_t^\phi, \quad (14)$$

where superscripts h and ϕ correspond to the hydrophilic and hydrophobic domains, respectively.

For sufficiently long hydrophobic stripes, the thin film should grow as an unperturbed finger, with leading and trailing edge velocities v_l and v_t , respectively. Disregarding the transient relaxation to these values, it is reason-

able to assume that the contact line changes its velocity instantaneously to v_l and v_t as soon as it comes into contact with a hydrophobic stripe. From this assumption, it follows that the residence time of the leading and trailing edges of the film in a hydrophobic stripe are

$$\Delta t_l^\phi = \frac{l_\phi}{v_l} \quad \text{and} \quad \Delta t_t^\phi = \frac{l_\phi}{v_t}.$$

For the hydrophilic stripes, we can write similar expressions for the residence times of the leading and trailing edges of the interface in a hydrophilic stripe,

$$\Delta t_l^h = \frac{l_h}{v_l^h} \quad \text{and} \quad \Delta t_t^h = \frac{l_h}{v_t^h}.$$

The velocity v_l^h corresponds to the mean velocity of the leading edge on a hydrophilic stripe, while v_t^h is defined as the velocity of the jump that the trailing interface undergoes on a prewet hydrophilic stripe.

To estimate v_l^h , we first approximate the volumetric flux supplied by the finger to the hydrophilic stripe as $\dot{q}_l \sim h_f \lambda W v_l$, where h_f and λW are the thickness and width of the finger in the hydrophobic stripe, respectively (see Fig. 2). The flow rate \dot{q}_l sustains the spreading of the leading edge, which covers a volume $V_l \simeq h_f l_h \hat{w}_h W$ of the hydrophilic stripe before it moves over the next hydrophobic stripe. The volume V_l depends on \hat{w}_h , which is the lateral fraction of the stripe that the film covers before the leading edge advances over the next hydrophobic domain. In writing the expression for V_l we have assumed that the film thickness does not vary significantly during spreading. The residence time of the spreading process is therefore $\Delta t_l^h = V_l / \dot{q}_l$, which gives a mean spreading velocity

$$v_l^h \simeq \frac{l_h}{\Delta t_l^h} = \frac{\lambda}{\hat{w}_h} v_l. \quad (15)$$

We next estimate the jumping velocity of the trailing edge, v_t^h . This velocity corresponds to the ratio between the length of the hydrophilic stripe, l_h , and the waiting time to observe the jump in the contact line position, Δt_t^h . Let h_t be the thickness of the trailing edge of the film when it touches the hydrophilic stripe, which is already wet and has a local thickness $h = h_t^0$, as shown in Fig. 2. After contact, the cross section of the film in the $x - z$ plane will evolve as $A_t^h \simeq h l_h = h_t^0 l_h + \dot{q}_t t$, where the flow rate per unit length in the y direction, \dot{q}_t , obeys $\dot{q}_t \sim v_t h_t$. We expect that A_t^h grows until the thickness of the film is $h = h_t$, from which it follows that the corresponding waiting time is

$$\Delta t_t^h = \frac{(h_t - h_t^0) l_h}{v_t h_t}. \quad (16)$$

We thus obtain an estimate for the jumping velocity of the trailing edge,

$$\hat{v}_t^h = \frac{v_t}{1 - \hat{h}_t}, \quad (17)$$

where $\hat{h}_t = h_t^0/h_t$.

We now return to Eq. (14), which we write in terms of the mean velocities of the leading and trailing edges, \hat{v}_l and \hat{v}_t , *i.e.*,

$$\frac{l_\phi + l_h}{\hat{v}_l} = \frac{l_h}{v_l^h} + \frac{l_\phi}{v_l} \quad \text{and} \quad \frac{l_\phi + l_h}{\hat{v}_t} = \frac{l_h}{v_t^h} + \frac{l_\phi}{v_t}. \quad (18)$$

From Eq. (18) we obtain the mean velocities of the interface as a function of the local velocities and the fraction of hydrophilic stripes,

$$\hat{v}_l = \frac{v_l}{1 + f \left(\frac{v_l}{v_l^h} - 1 \right)} \quad \text{and} \quad \hat{v}_t = \frac{v_t}{1 + f \left(\frac{v_t}{v_t^h} - 1 \right)}, \quad (19)$$

where v_l and v_t can be measured from the single finger solution, while v_l^h and v_t^h follow from Eqs. (15) and (17). For the leading edge velocity we obtain

$$\hat{v}_l = \frac{v_l}{1 + f \left(\frac{\hat{w}_h}{\lambda} - 1 \right)}, \quad (20)$$

which is proportional to the leading edge velocity of the finger and depends on the fraction of hydrophilic stripes, as well as on the degree of transverse spreading, which is contained in the dependence on \hat{w}_h .

For the trailing edge velocity we find

$$\hat{v}_t = \frac{v_t}{1 - \hat{h}_t f}, \quad (21)$$

which is controlled by the local thickness of the film on the prewet hydrophilic stripe.

Equations (20) and (21) can be used to obtain the growth rate of the contact line,

$$\dot{L} = \hat{v}_l - \hat{v}_t = \frac{v_l}{1 + f \left(\frac{\hat{w}_h}{\lambda} - 1 \right)} - \frac{v_t}{1 - \hat{h}_t f}. \quad (22)$$

In order to verify the validity of Eq. (22), values of λ , v_f , v_t , \hat{w}_h , and \hat{h}_t have to be provided. The finger width, λ , and the finger velocities of the leading and trailing edges, v_f , and v_t , are known from the finger growth on a homogeneous hydrophobic substrate. For our simulation parameters, $v_l = 1.1$, $v_t = 0.6$, and $\lambda \simeq 0.3$ as measured from the finger solution ($f = 0$). On the other hand, \hat{h}_t and \hat{w}_h are geometrical parameters that can be measured from simulations. We find that \hat{h}_t does not depend on the length or on the fraction of hydrophilic domains and we measure $\hat{h}_t = 0.33$. In contrast, \hat{w}_h shows a dependence on l_h , which is essentially controlled by the competition between the forward motion of the film the lateral spreading caused by the hydrophobic covering. For long hydrophilic domains, the film spreads to a larger extent before the leading edge arrives to the next hydrophobic domain. Therefore, \hat{w}_h increases with l_h . This introduces the dependence of the growth rate on l_h . We do not have a prediction for \hat{w}_h as a function of l_h . Instead, we measure these values from our simulations. For the runs performed we find $\hat{w}_h = 0.58$ for $l_h/x_c = 1.3$, $\hat{w}_h = 0.60$ for $l_h/x_c = 4.0$, and $\hat{w}_h = 0.64$ for $l_h/x_c = 6.7$.

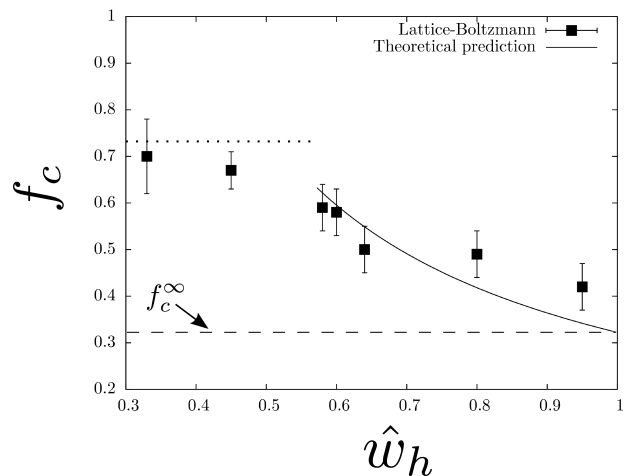


FIG. 5: Critical fraction, f_c , as a function of the fraction of the hydrophilic stripe covered by the leading edge, \hat{w}_h . The fraction \hat{w}_h increases with the length of the hydrophilic stripes, l_h . Lattice-Boltzmann simulations (solid symbols) show that the critical fraction decreases substantially with increasing \hat{w}_h , *i.e.*, with increasing l_h . This behavior is captured by a kinematical model for large \hat{w}_h , depicted by the solid line (see text).

In Figure 4 we show a comparison of Eq. (22) with simulation results. As depicted in the figure, the theoretical prediction captures the main dependence of the growth rate of the contact line, \dot{L} , both on f and, through \hat{w}_h , on l_h . For a fixed hydrophilic domain length, l_h , \dot{L} decreases with increasing f due both to a decrease of the leading edge velocity, as shown by Eq. (20), and by an increase of the trailing edge velocity, as predicted by Eq. (21). On the other hand, for fixed f , increasing l_h has the effect of decreasing the growth rate. This effect can be traced back to Eq. (15), which shows that increasing \hat{w}_h has the effect of slowing down the leading edge on a hydrophilic domain.

The theoretical result given by Eq. (22) predicts a critical fraction of hydrophilic stripes, $f_c < 1$, above which the growth rate, \dot{L} , vanishes. Such a saturation emerges both from the decrease of the leading edge velocity and the increase of the trailing edge velocity, an effect that is intimately linked to the fraction of hydrophilic stripes imposed to the substrate. The critical fraction follows from setting $\dot{L} = 0$ in Eq. (22), and reads

$$f_c = (v_l - v_t) \left[v_l \hat{h}_t + v_t \left(\frac{\hat{w}_h}{\lambda} - 1 \right) \right]^{-1}. \quad (23)$$

Here, the relevant dependence is $f_c(\hat{w}_h)$, given that \hat{w}_h can be controlled by choosing the length of the hydrophilic domains l_h .

In Fig. 5 we show a plot of f_c as a function of l_h and \hat{w}_h . We have included f_c data for four additional values of l_h ; $l_h/x_c = 0.4$, $l_h/x_c = 0.7$, $l_h/x_c = 10.1$ and $l_h = 13.4$. Corresponding values of \hat{w}_h are $\hat{w}_h = 0.33$, $\hat{w}_h = 0.45$, $\hat{w}_h = 0.80$ and $\hat{w}_h = 0.95$, respectively. We also show the

theoretical prediction given by Eq. (23), which accurately captures the decrease of f_c as \hat{w}_h increases for large \hat{w}_h .

An interesting limit corresponds to short hydrophilic domains, which we can include in our theory. As shown in the figure, the critical fraction reaches a saturation value, which originates from a weaker lateral spreading. In this limit the lateral size of the film in a hydrophilic domain remains close to the width of the finger, *i.e.*, $\hat{w}_h \simeq \lambda$. Still, the hydrophilic interaction causes a decrease in the local contact angle. As the leading edge encounters the next hydrophobic boundary, the capillary ridge grows, until the contact angle reaches the advancing contact angle of the hydrophobic stripe. The relevant timescale is given by the filling of the capillary ridge, which we approximate as a spherical cap of radius $R \simeq h_f/2$ and volume $V_l = 2\pi(h_f/2)^3/3$. The volumetric flow coming into the sphere still obeys $\dot{q}_l = h_f\lambda W v_l$. Adding this contribution to the residence time, we find the spreading-filling velocity,

$$v_l^h(\hat{w}_h \rightarrow \lambda) = \frac{v_l}{\frac{\pi h_f^2}{6\pi\lambda W l_h} + \frac{\hat{w}_h}{\lambda}}. \quad (24)$$

Eq. (24) can be used to obtain the critical fraction in this limit, which reads

$$f_c(\hat{w}_h \rightarrow \lambda) = (v_l - v_t) \left[v_l \hat{h}_t + v_t \left(\frac{\pi h_f^2}{6\pi\lambda W l_h^*} \right) \right]^{-1}, \quad (25)$$

where l_h^* is the crossover hydrophilic stripe length below which filling dominates over spreading. The dotted line in Fig. 5 shows the value predicted by Eq. (25) for $l_h^*/x_c \approx 0.4$, which is a typical stripe length for which no lateral spreading is observed. As depicted in the figure, this limiting value reasonably captures the saturation of the critical fraction for small \hat{w}_h . It is important to remark that the estimate of the leading edge velocity given by Eq. (24) is expected to be valid only as $\hat{w}_h \rightarrow \lambda$; for larger \hat{w}_h , the shape of the leading ridge is expected to depend on \hat{w}_h . Still, the filling timescale is subdominant, as shown by the good agreement of simulation data with Eq. (23), and we thus disregard it.

The opposite case, corresponding to $\hat{w}_h \rightarrow 1$, is an interesting regime, as in this case the imposed pattern has the smallest critical fraction of hydrophilic stripes for which saturation is expected. In this limit the leading edge spreads completely in the transverse direction on a hydrophilic stripe, a situation favored by long hydrophilic domains. In Eq. (23), this is equivalent to setting $\hat{w}_h = 1$, from which it follows that the minimum possible critical fraction is

$$f_c^\infty = (v_l - v_t) \left[v_l \hat{h}_t + \left(\frac{1}{\lambda} - 1 \right) v_t \right]^{-1}. \quad (26)$$

For the simulation values used in this work we find $f_c^\infty \simeq 0.3$. In Fig. 5(b) we plot this value, which is a good estimate of the limiting critical fraction as suggested by

Lattice-Boltzmann results. While both simulation and theory predict a slow final decay towards the limiting critical fraction, there is a rapid variation for intermediate stripe lengths, as shown in Fig. 5. For example, for $l_h/x_c = 13.4$ we obtain $f_c \simeq 0.4$. This value of the stripe length should be compared to the typical finger spacing, which for our simulations is $\Lambda_{max}/x_c = 8$. Therefore, one expects critical fractions significantly smaller than unity for stripes whose length is comparable to the lengthscale of the unstable film.

V. CONCLUSIONS

By means of Lattice-Boltzmann simulations and analytical approximations, we have studied the effect of heterogeneous hydrophilic-hydrophobic substrates composed of transverse striped patterns on the dynamics of forced thin liquid films, and have demonstrated that the film growth can be controlled by the interaction of the film with a prescribed hydrophilic-hydrophobic pattern.

We have focused on a scenario where the unstable contact line gives rise to sawtooth and finger structures on homogeneous hydrophilic and hydrophobic substrates, respectively, and have examined how the growth of the contact line is altered by the chemical pattern. To this end, we have considered patterns where the typical lengthscale is comparable to the most unstable wavelength of the contact line, Λ_{max} .

For the transverse striped patterns considered, we have shown that above a critical fraction of hydrophilic stripes, f_c , the saturation of the film is achieved. The mechanism that causes such a saturation originates from transverse spreading of the leading edge of the contact line on the hydrophilic domains and from the growth of the film at the hydrophilic-hydrophobic boundary so as to reach the advancing contact angle. These processes contribute to a reduction of the velocity of the leading edge. As this occurs, a film of fluid is left on the hydrophilic domains, thus increasing the velocity of the trailing edge as soon as it comes into contact with a hydrophilic stripe, which already has been wet. The trailing edge jumps every time it finds a wet domain, with the corresponding gain in the trailing edge velocity. The global outcome is that for sufficiently large fractions of hydrophilic stripes, the net growth rate of contact line vanishes, independently of the details of the dynamics of the contact line.

We have captured this effect with a kinematical model, assuming local relaxation of the leading and trailing edge velocities to ‘hydrophilic’ and ‘hydrophobic’ values. Hydrophobic values have been approximated as the velocities of the leading and trailing edges of an unperturbed finger, while the hydrophilic velocity values have been estimated by mass conservation. The global growth rate of the contact line, \dot{L} , has been determined by the difference of the mean velocities of the leading and trailing edges of the contact line. By estimating these velocities on kinematical grounds, we have obtained a prediction

for the global growth rate, which is given by Eq. (22). We have estimated the critical fraction, f_c , at which saturation occurs indirectly as a function of the length of the hydrophilic domains, given by Eq. (23). For long hydrophilic domains, in which transverse spreading is more efficient, we find a good agreement between the simulation results and the theoretical prediction. In this limit, we have estimated the minimum fraction of hydrophilic stripes for which saturation is expected, which for the simulation parameters considered in this work is as low as $f_c \simeq 0.3$. However, experimentally feasible domain lengths, comparable to the length scale of the growing fingers, give critical fractions of about $f_c = 0.6$ to $f_c = 0.7$, still considerably smaller than unity.

Our theoretical prediction, given by Eq. (23) can be used to estimate the critical fraction of hydrophilic stripes above which the saturation of the contact line is expected. To examine the reliability of our approach in a real system we consider a potential microfluidic device where a water film of thickness $h_c = 10 \mu\text{m}$ is forced on a micropattern in the presence of air. The air-water pair closely reproduces the viscosity contrast used in the simulations. Our simulations show that the instability is effectively suppressed using a sharp contrast in the wetting properties between the domains forming the micropattern. For example, a front moving over a Polymethyl methacrylate (PMMA) substrate would have a relatively large contact angle ($\theta_e \approx 74^\circ$), where fingers are expected to develop [9]. In that case, the low-wetting angle domains could be formed using glass ($\theta_e \approx 25^\circ$) or a gold coating ($\theta_e \approx 0^\circ$) [32].

Microfluidic devices operate over a wide range of velocities, covering from $\mu\text{m/s}$ to cm/s [33]. Here we consider an injection velocity of $u = 1 \text{ mm/s}$ as a representative example. Under these circumstances, the required body force to drive the film follows from the force balance far from the contact line, $f_x = 3\eta_1 u/h_c^2 \sim 10^4 \text{ Pa/m}$. Such body forces are of the order of the gravitational force density for water and can be accomplished by simple column devices and accurately controlled by syringe pumps. From our simulation measurements we estimate the leading and trailing edge velocities of steady finger

propagating at the imposed speed on a hydrophobic substrate, $v_l \approx 1.1 \text{ mm/s}$ and $v_r \approx 0.6 \text{ mm/s}$. Our prediction shows that the film will saturate at a different fraction of hydrophilic coverage depending on the width of the hydrophilic stripes, l_h , which determines the fraction of lateral spreading, \hat{w}_h . A sensible choice is to set l_h to the order of magnitude of the lengthscale of the instability, $x_c = h_c(3Ca)^{-1/3}$. Thus, for $l_h = x_c \sim 10^2 \mu\text{m}$, we get the spreading fraction $\hat{w}_h \approx 0.58$. Using this value of w_h and comparing with Fig. 4, the film is expected to saturate at a critical fraction $f_c \approx 0.6$.

The previous example shows the experimental feasibility of the mechanisms proposed in this work for a regular liquid under typical conditions found in microfluidics. However, the fact that the relevant length scale with the film thickness (expressed here by the choice of units to report our results) indicates that a proper up- or down-scaling of the system size and the applied forcing can provide a substantial flexibility to induce analogous phenomena in different liquid/gas or liquid/liquid mixtures at scales below the capillary length. This opens the possibility of a better control of the fingering instability in controlled environments by substrate heterogeneity. Our approach relies on chemical patterning, which has already been explored experimentally, even at the microscale. We therefore expect our results to motivate further experimental investigations, with potential impact in microfluidic technologies.

VI. ACKNOWLEDGMENTS

R.L.-A. wishes to thank M. Pradas for useful discussions. We acknowledge financial support from Dirección General de Investigación (Spain) under projects FIS 2009-12964-C05-02, FIS 2008-04386, and DURSI projects SGR2009-00014 and SGR2009-634. R.L.-A. acknowledges support from CONACyT (México) and Fundación Carolina (Spain). The computational work presented herein has been carried out in the MareNostrum Supercomputer at Barcelona Supercomputing Center.

-
- [1] R.V. Craster and O.K. Matar. Dynamics and stability of thin liquid films. *Rev. Mod. Phys.*, 81:1131, 2009.
 - [2] A. Oron, S. H. Davis, and S. G. Bankoff. Long-scale evolution of thin liquid films. *Rev. Mod. Phys.*, 69:931, 1997.
 - [3] Markus Rauscher, S. Dietrich, , and Joel Koplik. Shear flow pumping in open micro- and nanofluidic systems. *Phys. Rev. Lett.*, 98:224504, 2007.
 - [4] D.E. Kataoka and S.M. Troian. Patterning liquid flow on the microscopic scale. *Nature*, 402:794, 1999.
 - [5] L. Kondic and J. Diez. Flow of thin films on patterned surfaces: Controlling the instability. *Phys. Rev. E*, 65(4):045301, 2002.
 - [6] Lou Kondic and Javier Diez. Instabilities in the flow of thin films on heterogeneous surfaces. *Phys. Fluids*, 16(9):3341–3360, 2004.
 - [7] Y. Zhao and J.S. Marshall. Dynamics of driven liquid films on heterogeneous surfaces. *J. Fluid Mech.*, 559:355, 2006.
 - [8] J.S. Marshall and S. Wang. Contact-line fingering and rivulet formation in the presence of surface contamination. *Comput. Fluids*, 34:664, 2005.
 - [9] R. Ledesma-Aguilar, A. Hernández-Machado, and I. Pagonabarraga. Dynamics of three-dimensional thin films: from hydrophilic to super-hydrophobic regimes. *Phys. Fluids*, 20:072101, 2008.
 - [10] B. M. Mognetti and J. M. Yeomans. Using electrowetting to control interface motion in patterned microchannels.

- Soft Matter*, 6:2400, 2010.
- [11] M. P. Brenner. Instability mechanism at driven contact lines. *Phys. Rev. E*, 47:4597, 1993.
- [12] S. M. Troian, X. L. Wu, and S. A. Safran. Fingering instability in thin wetting films. *Phys. Rev. Lett.*, 62:1496–1499, 1989.
- [13] J.M. Davis and S.M. Troian. On a generalized approach to the linear stability of spatially non-uniform thin film flows. *Phys. Fluids*, 15:1344, 2003.
- [14] S. M. Troian, E. Herbolzheimer, S. A. Safran, and J.F. Joanny. Fingering instabilities in driven spreading films. *Europhys. Lett.*, 10:25–30, 1989.
- [15] H.E. Huppert. The flow and instability of viscous gravity currents down a slope. *Nature*, 300:427, 1982.
- [16] N. Silvi and E.B. Dussan. On the rewetting of an inclined solid surface by a liquid. *Phys. Fluids*, 28:5–7, 1985.
- [17] J.R. de Bruyn. Growth of fingers at a driven three-phase contact line. *Phys. Rev. A*, 46:R4500, 1992.
- [18] K.E. Holloway, P. Habdas, N. Semsarillar, K. Burfitt, and J.R. de Bruyn. Spreading and fingering in spin coating. *Phys. Rev. E*, 75:046308, 2006.
- [19] F.J. Higuera, S. Succi, and R. Benzi. Lattice gas-dynamics with enhanced collisions. *Europhys. Lett.*, 9:345, 1989.
- [20] M.R. Swift, E. Orlandini, W.R. Osborn, and J. Yeomans. Lattice boltzmann simulation of liquid-gas and binary fluid systems. *Phys. Rev. E*, 54:5041, 1996.
- [21] A. Moosavi, M. Rauscher, and S. Detrich. Motion of nanodroplets near chemical heterogeneities. *Langmuir*, 24:734, 2008.
- [22] R. Ledesma-Aguilar, A. Hernández-Machado, and I. Pagonabarraga. Three-dimensional aspects of fluid flows in channels: I. Meniscus and thin film regimes. *Phys. Fluids*, 19:102112, 2007.
- [23] V. M. Kendon, M. E. Cates, I. Pagonabarraga, J. C. Desplat, and P. Bladon. Inertial effects in three-dimensional spinodal decomposition of a symmetric binary mixture: a Lattice-Boltzmann study. *J. Fluid Mech.*, 440:147–203, 2001.
- [24] C. Huh and L.E. Scriven. Hydrodynamic model of steady movement of a solid/liquid/fluid contact line. *J. Colloid Interface Sci.*, 35:85, 1971.
- [25] T. Qian, X.-P. Wang, and P. Sheng. A variational approach to moving contact line hydrodynamics. *J. Fluid Mech.*, 564:333, 2006.
- [26] A.J. Briant and J.M. Yeomans. Lattice Boltzmann simulations of contact line motion. II. Binary fluids. *Phys. Rev. E*, 69:031603, 2004.
- [27] D. Bonn, J. Eggers, J. Indekeu, J. Meunier, and E. Rolley. Wetting and spreading. *Rev. Mod. Phys.*, 81:739, 2009.
- [28] A.J. Bray. Theory of phase ordering-kinetics. *Adv. Phys.*, 43:357–459, 1994.
- [29] M.E. Cates, J.-C. Desplat, P. Stansell, A.J. Wagner, K. Stratford, R. Adhikari, and I Pagonabarraga. Physical and computational scaling issues in lattice Boltzmann simulations of binary fluid mixtures. *J. Stat. Phys.*, 363:1917, 2005.
- [30] A.C.J. Ladd and R. Verberg. Lattice-Boltzmann simulations of particle-fluid suspensions. *J. Stat. Phys.*, 104:1191–1251, 2001.
- [31] J. C. Desplat, I. Pagonabarraga, and P. Bladon. Ludwig: A parallel Lattice-Boltzmann code for complex fluids. *Comp. Phys. Comm.*, 134:273–290, 2001.
- [32] H. Bruus. *Theoretical Microfluidics*. Oxford University Press, 2008.
- [33] T.M. Squires and S.R. Quake. Microfluidics: Fluid physics at the nanoliter scale. *Rev. Mod. Phys.*, 77:3, 2005.